ChemPubSoc Europe
DOI: 10.1002/chem.201405043
CHEMISTRY
A European Journal
Full Paper

NMR Spectroscopy

Natural Abundance ^{15}N NMR by Dynamic Nuclear Polarization: Fast Analysis of Binding Sites of a Novel Amine-Carboxyl-Linked Immobilized Dirhodium Catalyst

Torsten Gutmann,*[a] Jiquan Liu,[a] Niels Rothermel,[a] Yeping Xu,[a] Eva Jaumann,[a] Mayke Werner,[a] Hergen Breitzke,[a] Snorri T. Sigurdsson,[b] and Gerd Buntkowsky*[a]

Abstract: A novel heterogeneous dirhodium catalyst has been synthesized. This stable catalyst is constructed from dirhodium acetate dimer ($Rh_2(OAc)_4$) units, which are covalently linked to amine- and carboxyl-bifunctionalized mesoporous silica (SBA-15–NH_2–COOH). It shows good efficiency in catalyzing the cyclopropanation reaction of styrene and ethyl diazoacetate (EDA) forming *cis*- and *trans*-1-ethoxycarbonyl-2-phenylcyclopropane. To characterize the structure of this catalyst and to confirm the successful immobilization, heteronuclear solid-state NMR experiments have been performed. The high application potential of dynamic nuclear polarization (DNP) NMR for the analysis of binding sites in this novel catalyst is demonstrated. Signal-enhanced ^{13}C CP MAS and ^{15}N CP MAS techniques have been employed to detect different carboxyl and amine binding sites in natural abundance on a fast time scale. The interpretation of the experimental chemical shift values for different binding sites has been corroborated by quantum chemical calculations on dirhodium model complexes.

Introduction

Dirhodium(II) complexes are a group of multinuclear compounds with structures containing an Rh–Rh bond and four bridging ligand moieties at equatorial positions (Figure 1 a). Such complexes have been successfully applied as highly efficient catalysts in organic chemistry to produce intermediates in drug synthesis by formation of carbon-carbon or carbon-heteroatom bonds through the generation of metallocarbenes.[1,2] However, their technical application potential is limited by recycling and recovery problems, and especially by the strict legislation concerning metal contaminations in pharmaceutical ingredients. Aiming at a more sustainable chemistry, there have been extensive investigations towards the development of recyclable heterogeneous dirhodium catalysts.[3] One technique for preparing heterogeneous catalysts is to immobilize the dirhodium complex by covalent grafting on functionalized silica or polymer supports. Various studies have focused on heterogenization at axial coordination sites (Figure 1 b) through amine or pyridine linkers, which offers an efficient means of anchoring different dirhodium complexes, including chiral ones.[3–8] Alternatively, heterogenization may be achieved by ligand exchange (Figure 1 c), although only a few examples of this have been reported. In this case, at

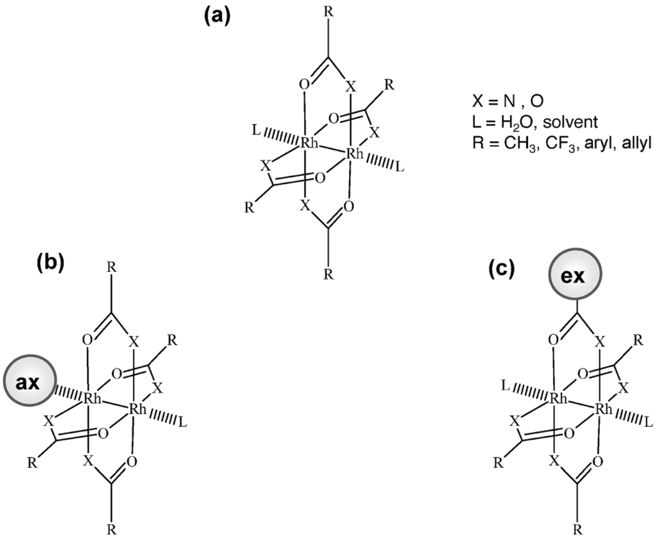

Figure 1. (a) General structure of dirhodium(II) complexes with carboxylate or carboxamide bridging ligands. Schematic representation of binding modes for immobilization of dirhodium(II) complexes: (b) axial coordination (ax), (c) ligand exchange (ex).

---

[a] T. Gutmann,+ J. Liu,+ N. Rothermel, Y. Xu, E. Jaumann, M. Werner, H. Breitzke, G. Buntkowsky
Institute of Physical Chemistry, Technical University Darmstadt
Alarich-Weiss-Straße 8, 64287 Darmstadt (Germany)
E-mail: gutmann@chemie.tu-darmstadt.de
gerd.buntkowsky@chemie.tu-darmstadt.de

[b] S. T. Sigurdsson
University of Iceland, Department of Chemistry, Science Institute
Dunhagi 3, IS-107 Reykjavík (Iceland)

[+] These authors contributed equally to this work.

Supporting information for this article is available on the WWW under http://dx.doi.org/10.1002/chem.201405043.

least one ligand of the original homogeneous dirhodium complex is exchanged with a carboxyl group of the functionalized silica or polymer.[9–11]

In the last decade, many types of silica-based transition metal catalysts with various functional groups, such as phosphorus-, thiol-, nitrogen-, and oxygen-containing linker molecules, have been synthesized and applied in catalysis.[12–33] For the rational development of this novel class of heterogeneous catalysts, it is crucial to obtain detailed information on both their successful immobilization and their binding sites in order to understand their catalytic behavior and potential stability in reactions. In principle, this analysis can be realized by structure determination employing solid-state NMR techniques, as was shown by a series of studies aimed at characterizing the structure and binding sites of such catalysts.[34–44]

In the case of phosphorus-containing functionalized materials, this analysis can be efficiently performed by employing solid-state NMR techniques due to the 100% natural abundance, high relative sensitivity, and large gyromagnetic ratio of ^{31}P. These favorable properties allow the application of a broad range of techniques, such as standard cross-polarization (CP) experiments, *J*-resolved or INADEQUATE experiments,[45–47] or specific heteronuclear-correlation techniques (HETCOR) designed for structure determination of such catalysts.[48,49] The combination of solid-state NMR with quantum chemical calculations offers unique possibilities for a detailed characterization of binding sites at the molecular level.[50,51] However, if less favorable nuclei, such as ^{15}N in amine-containing linkers, are involved, the analysis of the binding sites becomes difficult due to the low abundance, low sensitivity, and low gyromagnetic ratio of the ^{15}N nucleus. In this case, selective ^{15}N isotopic labeling or at least isotope enrichment of the linker is mandatory to acquire an appropriate signal-to-noise ratio within a reasonable time. Hyperpolarization techniques such as parahydrogen-induced polarization (PHIP),[52–55] spin exchange by optical pumping (SEOP),[56–59] and dynamic nuclear polarization (DNP) are the methods of choice to overcome sensitivity problems in functionalized materials or heterogeneous catalyst systems.[60–63] However, to date, only a few studies have dealt with the detection of ^{15}N in natural abundance for analysis of heterogeneous catalysts employing DNP,[64,65] which has mainly been used to enhance the signals of ^{15}N for structure determination of functional materials[66–68] and in biologically relevant systems.[69–72]

The present work is focused on the ^{15}N and ^{13}C solid-state NMR characterization of a novel dirhodium catalyst immobilized on the surface of bifunctionalized mesoporous silica employing a combination of surface-enhanced DNP NMR with quantum chemical calculations to model the NMR parameters of the possible binding sites.

The article is structured as follows. After this brief introduction, the experimental and computational procedures are explained in detail. In the first part of the Results and Discussion section, the synthetic strategy for obtaining the heterogeneous dirhodium catalyst is outlined. It involves the rhodium acetate dimer ($Rh_2(OAc)_4$), which is immobilized on the surface of a bifunctionalized (amine and carboxyl) SBA-15-type material. In the main part, we discuss the characterization of the materials and catalysts employing conventional and/or DNP NMR spectroscopy. The experimental results are then interpreted in combination with theoretical results from DFT calculations. Finally, the activity of the new heterogeneous dirhodium catalyst (**3**) has been investigated for the cyclopropanation reaction of styrene and ethyl diazoacetate (EDA) forming *cis*- and *trans*-1-ethoxycarbonyl-2-phenylcyclopropane stereoisomers.

Experimental Section

Preparation of the support material and immobilization of the catalyst

SBA-15–NH$_2$–COOH (1): Bifunctionalized mesoporous silica **1** containing both amine and carboxyl groups was synthesized by co-condensation of (3-aminopropyl)triethoxysilane (APTES, 99% wt., Sigma–Aldrich) with carboxyethylsilanetriol sodium salt (CES, 25% vol., ABCR) following published procedures.[36,73] Typically, Pluronic P123 (4.0 g; Sigma–Aldrich) as a template was dissolved in 2 M aqueous HCl (120 mL) diluted with water (30 mL) under stirring at 40 °C. A mixture of tetraethyl orthosilicate (TEOS, 98% wt., 6.83 g, 0.0328 mol; Sigma–Aldrich), APTES (0.91 g, 0.0041 mol), and CES (2.86 g, 0.0041 mol) was added to the solution at 40 °C and stirred over a period of 20 h. After aging at 80 °C for 24 h without stirring, the solid product was recovered, washed, and air-dried at room temperature. The template was partly removed by soxhlet extraction with ethanol for 48 h. The obtained mesoporous silica was dried at 80 °C under vacuum to ensure complete removal of the solvent. The product showed a narrow pore size distribution with an average diameter of 3.8 nm. The BET surface area and pore volume were calculated as 435.02 $m^2 g^{-1}$ and 0.5561 $cm^3 g^{-1}$, respectively. Elemental analysis (wt.%): C 15.30, H 3.041, N 1.77.

SBA-15–NH$_2$ (2): Amine-functionalized mesoporous silica **2** was synthesized according to the same procedure as described for **1**, but employing only APTES (0.91 g, 0.0041 mol) and TEOS (7.69 g, 0.0369 mol). The product showed a narrow pore size distribution with an average diameter of 3.85 nm. The BET surface area and pore volume were calculated as 477.13 $m^2 g^{-1}$ and 0.5476 $cm^3 g^{-1}$, respectively. Elemental analysis (wt.%): C 4.504, H 3.206, N 1.33.

SBA-15–NH$_2$–COOH + Rh$_2$(OAc)$_4$ (3): The dirhodium catalyst was immobilized by wet impregnation after a heating step under vacuum. Rhodium acetate dimer (0.01 g) was dissolved in acetonitrile (1.25 mL) and the solution was used to impregnate bifunctional mesoporous silica **1** (1 g). After evaporation of the solvent at room temperature, a small amount of acetonitrile (ca. 0.5 mL) was added. This process was repeated five times. The air-dried solid was then heated at 80 °C under vacuum for 24 h to remove the side product (acetic acid). The catalyst was washed by soxhlet extraction with acetonitrile for 48 h to remove physisorbed and unbound dirhodium complex. Finally, the product was dried under vacuum to afford the heterogeneous catalyst as a grey-green powder. The obtained catalyst showed a decreased BET surface area of 229.88 $m^2 g^{-1}$ and a pore volume of 0.162 $cm^3 g^{-1}$. Elemental analysis (wt.%): C 12.19, H 3.087, N 1.679.

Solid-state NMR experiments without DNP

All room temperature solid-state NMR spectra were measured on a 500 MHz Varian Unity Inova spectrometer equipped with a Bruker 4 mm standard bore HX MAS probe. Spectra were recorded at frequencies of 125.81 MHz for ^{13}C and 99.36 MHz for ^{29}Si.

Cross-polarization (CP) experiments were performed with contact times of 3 ms for ^{13}C and ^{29}Si at a spinning rate of 6 kHz. Adequate signals were collected after overnight acquisition.

DNP-enhanced solid-state NMR experiments

For all DNP measurements 1-(TEMPO-4-oxy)-3-(TEMPO-4-amino)-propan-2-ol (TOTAPOL) was employed as a popularbiradical polarizing agent.[74] This radical was synthesized according to the procedure described by Song et al.[75] In a typical sample preparation, the functionalized material (10–15 mg) was wetted with a 0.015 M solution of TOTAPOL in D_2O/H_2O (90:10; 15 μL) and packed in a 3.2 mm sapphire rotor. All DNP-enhanced solid-state NMR experiments were performed on a Bruker Avance III 400 spectrometer system equipped with an Ascend^{TM} 400 DNP magnet, a low-temperature triple-resonance $^{1}H/X/Y$ probe, and a 9.7 T Bruker gyrotron system, corresponding to a microwave frequency of 263 GHz. Spectra were recorded at frequencies of 400.02 MHz for ^{1}H, 100.59 MHz for ^{13}C, and 40.53 MHz for ^{15}N for optimal matching with the microwave source. ^{13}C and ^{15}N spectra were measured at nominally 100 K at a spinning rate of 8 kHz. Cross-polarization (CP) experiments were performed with contact times of 2 ms for ^{13}C and 3 ms for ^{15}N, and a repetition delay of 10 s according to the approximate T_1 times of the protons in these samples at this temperature. 128 accumulations were performed for ^{13}C spectra (measurement time 21 min) and 5000 accumulations were performed for ^{15}N spectra (measurement time 14 h). During data acquisition, dipolar interactions with protons were decoupled employing two-pulse phase-modulated (TPPM) decoupling[76] with a 20° phase jump. All ^{13}C spectra were referenced to TMS, and ^{15}N spectra were referenced to CH_3NO_2 employing NH_4Cl as an external standard ($\delta = -341.168$ ppm[77]).

Activity test of the heterogeneous dirhodium catalyst

To test the activity of the SBA-15–NH_2–COOH + $Rh_2(OAc)_4$ (**3**) catalyst, the cyclopropanation of ethyl diazoacetate (EDA) with styrene was investigated as a model reaction.[7] In a typical procedure, styrene (1.04 g) was added to a suspension of the catalyst (0.075 g) in CH_2Cl_2 (6.65 g), and the mixture was subjected to ultrasonic dispersion for 15 min. A solution of EDA (0.058 g) in CH_2Cl_2 (2 g) was then added and the mixture was stirred at room temperature. Samples were taken after 15 min, 1 h, 2 h, 3 h, 4 h, and 5 h and analyzed on a gas chromatograph (GC) (Agilent Technologies 7820 A), which was equipped with an HP-5 column (30 m × 0.32 mm × 0.25 μm) and an FID detector. For separation of the stereoisomers, a GC temperature program of initially 80 °C with an 8 °C min^{-1} ramp for 3 min followed by a 15 °C min^{-1} ramp for 8 min was selected, at an N_2 gas flow of 1.4 mL min^{-1}. The retention times for the *cis* and *trans* isomers were then 8.2 min and 8.6 min, respectively.

Computational details

All DFT calculations were carried out with the Orca program system.[78] Model structures for the coordination of amine linkers to $Rh_2(OAc)_4$ were created from the crystal structure of $Rh_2(OAc)_4(H_2O)_2$,[79] replacing one (structure **I**) or two (structure **II**) of the water molecules by propylamine. Geometry optimization was performed with Becke's three-parameter hybrid functional[80,81] along with the Lee–Yang–Parr correlation functional (B3LYP)[82] and Pople's double-ζ basis set 6-31G(d,p) combining d- and p-polarization functions.[83,84] In these optimization runs, the core electrons of Rh were replaced by the fully relativistic effective core potential (ECP) developed by the Stuttgart group.[85] The ^{15}N chemical shieldings were calculated at the same level of theory employing the triple-ζ basis set 6-311++G(3df,3dp) including four sets of polarization functions and additional diffuse functions on all atoms.[83,84,86–88] For easier assignment of the ^{13}C signals of the support material SBA-15–NH_2–COOH (**1**), chemical shift predictions based on atomic increment algorithms were arranged employing the ACD Labs software package.

Results and Discussion

Synthesis and basic characterization of the immobilized dirhodium catalyst

Before the immobilization of the homogeneous dirhodium catalyst, the bifunctionalized support material SBA-15–NH_2–COOH (**1**) had to be synthesized. The synthetic procedure followed a slightly modified version of the co-condensation[36] to achieve a relatively homogeneous distribution of carboxyl and amine groups on the surface of the mesoporous material. According to the N_2 adsorption–desorption isotherms of the support material (see Supporting Information, Figure S0a), the type IV isotherm with H1 hysteresis in the mesopore range demonstrated the presence of open-ended cylindrical mesopores, which is a feature of SBA-15-type mesoporous matrices.

This supporting material was then used to graft the homogeneous dirhodium complex in two steps. In the wet impregnation step, which was performed at room temperature, an amine group coordinates at an axial site of the Lewis acidic dirhodium complex.[7] In the second heating step under vacuum, carboxyl groups on the surface of the mesoporous silica undergo ligand exchange with the dirhodium complex. Following this synthetic protocol, it can be assumed that the dirhodium complex is attached to the surface through both amine and carboxyl functions. The immobilized catalyst displayed a type IV isotherm, but, in contrast to the support material, it showed H3 hysteresis (see Supporting Information Figure S0b). The pore size distribution became broader and the average diameter of the pores decreased. This further suggested that the dirhodium complex was deposited in the mesopores after immobilization.

Solid-state NMR characterization

^{29}Si solid-state NMR

To characterize the surface of the SBA-15–NH_2–COOH (**1**) support material, ^{29}Si CP-MAS NMR spectra were recorded (Figure 2). The three signals at $\delta = -99$, -106, and -114 ppm were assigned to the silicon atoms of silanol groups labeled as Q_2, Q_3, and Q_4 present on the surface.[34,36,89] Structural changes on the silica surface due to the binding of amine and carboxyl linkers are revealed by the appearance of T_n signals ($\delta = -66$ and -72 ppm). These signals are consistent with reaction of the APTES and CES linkers with TEOS during the co-condensation process, forming one, two, or three –Si–O–Si– bonds. This confirmed the successful functionalization of the surface through covalent bonding. Interestingly, in contrast to previously published data for SiO_2 nanoparticles[89] or functionalized

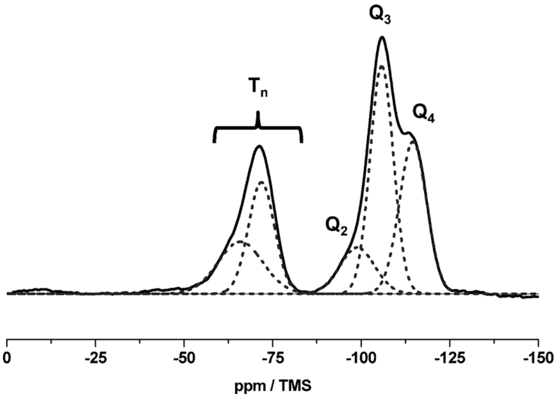

Figure 2. ^{29}Si CP MAS spectrum of the bifunctionalized SBA-15–NH_2–COOH (**1**) material at 6 kHz spinning. The observation of T_n groups confirms the successful functionalization of the SBA-15 material.

SBA-3 material,[34] only two resolvable signals were observed. We assume that this phenomenon results from the co-condensation method employed for the preparation.

After immobilization of the $Rh_2(OAc)_4$ catalyst, the ^{29}Si CP MAS spectrum (see Supporting Information Figure S1) remained essentially unchanged, as previously observed for a Wilkinson-type catalyst immobilized on functionalized SBA-3 material.[34] This shows that the rhodium has no significant influence on the chemical environment of the silica and, furthermore, that the stability of the material is not compromised by the metal.

^{13}C solid-state DNP NMR

Figure 3a shows the ^{13}C NMR spectrum of the support material **1** recorded under microwave irradiation. From this spectrum, it is evident that the SBA-15 material contained two different types of linker molecules, namely the CES linker represented by the characteristic chemical shift of the CO group at around 180 ppm and two signals in the aliphatic region, and the APTES linker represented by three signals in the aliphatic region. From the prediction of ^{13}C NMR chemical shifts by atomic increment-based algorithms, one can assume that the signals at $\delta = 8.9$, 21.1, and 42.2 ppm are due to the APTES linker, whereas those at $\delta = 13.8$ and 29.5 ppm are due to the CES linker. Interestingly, the broad signal at $\delta = 180$ ppm consists of two overlapping signals (Figure 3a, inset), one at 183.3 ppm and the other at 178.0 ppm. This observation suggests that besides the carboxyl function, expected to be responsible for the signal at $\delta = 183.3$ ppm, the sample also contains an amide function, giving rise to the upfield-shifted ^{13}C signal at $\delta = 178.0$ ppm. In addition to these signals, a group of signals centered at $\delta = 70$ ppm can be discerned, which can be ascribed to template molecules that were not completely removed during the synthesis.

After immobilization of the $Rh_2(OAc)_4$, the ^{13}C CP MAS spectrum was modified by the appearance of additional small overlapping signals in the aliphatic region (Figure 3b). These can be assigned to the acetate ligands of $Rh_2(OAc)_4$. In the carbonyl group region, a third superimposed signal appears at $\delta = 190.5$ ppm (Figure 3b, inset), which clearly indicates carboxyl functions coordinated to the rhodium centers. A similar chemical shift is also seen for the neat crystalline $Rh_2(OAc)_4$ catalyst (see Supporting Information, Figure S2). However, since unbound $Rh_2(OAc)_4$ is soluble in warm acetonitrile and should be removed from the surface by washing for 48 h, the new signal at $\delta = 190.5$ ppm can clearly be assigned to strongly bound catalyst on the surface (Figure 4a). To confirm this hypothesis, $Rh_2(OAc)_4$ was also grafted onto SBA-15–COOH containing only carboxyl linker groups. The recorded spectra (see Supporting Information Figure S3) demonstrated that after grafting of $Rh_2(OAc)_4$ and washing, a somewhat downfield-shifted signal was still visible, strongly indicating the presence of bound catalyst on the surface.

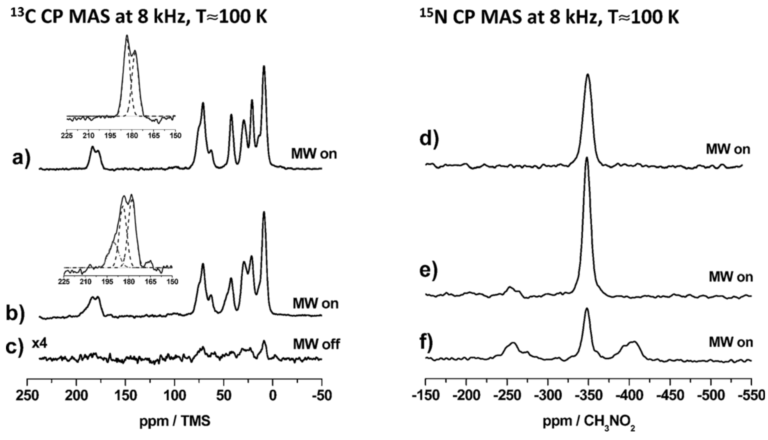

Figure 3. ^{13}C and ^{15}N NMR spectra measured at 8 kHz spinning rate at nominally 100 K: (a) ^{13}C CP MAS of SBA-15–NH_2–COOH (**1**) with MW on and deconvolution of the signals of the carbonyl functions, (b) ^{13}C CP MAS of SBA-15–NH_2–COOH + $Rh_2(OAc)_4$ (**3**) with MW on and deconvolution of the signals of the carbonyl functions, (c) ^{13}C CP MAS of SBA-15–NH_2–COOH + $Rh_2(OAc)_4$ (**3**) with MW off, (d) ^{15}N CP MAS of SBA-15–NH_2 (**2**) with MW on, (e) ^{15}N CP MAS of SBA-15–NH_2–COOH (**1**) with MW on, and (f) ^{15}N CP MAS of SBA-15–NH_2–COOH + $Rh_2(OAc)_4$ (**3**) with MW on.

^{15}N solid-state DNP NMR

Whereas the sensitivity of ^{13}C CP MAS spectroscopy is in principle high enough to record natural abundance ^{13}C spectra employing long acquisition times and signal averaging, this is not feasible for natural abundance ^{15}N CP MAS, since it is roughly two orders of magnitude less sensitive. Here, the sensitivity is limited by the low natural abundance (0.368 %) and the low gyromagnetic ratio ^{15}N (-2.7126×10^7 rad T^{-1} s^{-1}) of the ^{15}N nucleus. Thus, for standard solid-state NMR, isotopic labeling with ^{15}N would be required, which cannot be realiz-

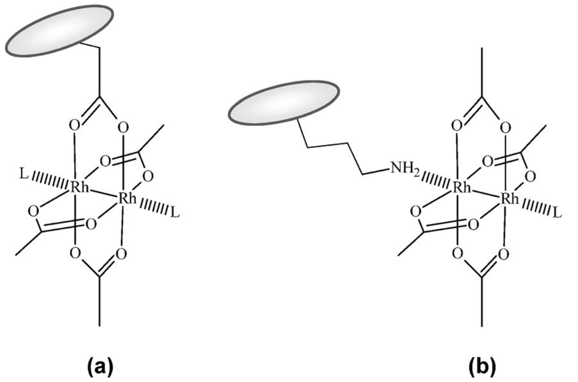

Figure 4. Possible binding modes for the immobilization of $Rh_2(OAc)_4$ derived from the ^{13}C and ^{15}N solid-state DNP NMR spectra: (a) ligand exchange of the carboxylate group and (b) axial coordination via the amine function.

ed with typical synthetic strategies for the investigated systems.

The ^{15}N CP MAS spectra measured with DNP (see Figure 3d–f) overcome these sensitivity problems. All spectra were acquired within measurement times of 14 h with an appropriate signal-to-noise ratio for unambiguous assignment of the signals. Figure 3d shows the spectrum of pure amino-functionalized SBA-15 material (**2**). The broad signal at $\delta=-349.0$ ppm corresponds to free amine functions, which display a wide distribution of isotropic chemical shifts due to their various chemical environments in the amorphous sample. When the SBA-15 material is functionalized with additional carboxyl linkers (**1**), the spectral line shape is slightly modified and a second signal appears at $\delta\approx-258$ ppm. Together with the signal at $\delta=178$ ppm in the ^{13}C NMR spectrum (see above), this second signal clearly demonstrates the presence of amide groups on the surface of the support material, which may result from the condensation of amine and carboxyl functions. In our systems, the formation of an amide or carbamide by reaction of a primary amine function with carbon dioxide[90,91] can be excluded, since such a reaction should also occur in the case of the pure amine-functionalized material (see Figure 3d).

After immobilization of $Rh_2(OAc)_4$ on **1**, the intensity of the signal at $\delta=-349.0$ ppm decreased and a new signal appeared at $\delta=-402.7$ ppm. This observation strongly indicates that the rhodium of the $Rh_2(OAc)_4$ catalyst is coordinated by the amine function of **1** as illustrated in Figure 4b.

Quantum chemical calculations

To support the assignment of the ^{15}N signals in the solid-state spectra, theoretical calculations were performed on model systems of $Rh_2(OAc)_4$. *n*-Propylamine (**III**) was chosen as a model ligand to simulate the coordination of the dirhodium complex by APTES-functionalized silica. Since we were only interested in isotropic chemical shift information, it seemed reasonable to neglect the silica part of the system to reduce computational costs. Moreover, the theoretical results could be readily compared with previous liquid-state NMR data.

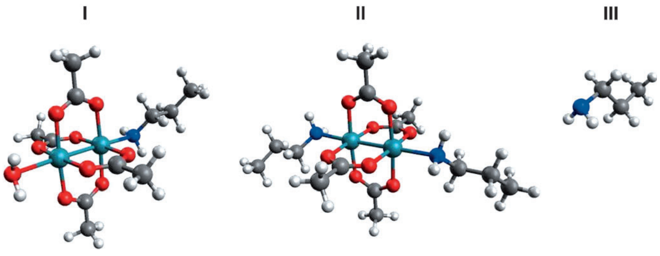

Figure 5. Structures for the NMR parameter calculations: *n*-propylamine-monosubstituted dirhodium complex (**I**), *n*-propylamine-disubstituted dirhodium complex (**II**), and *n*-propylamine (**III**).

Two different structures (see Figure 5) were created by replacing one (structure **I**) or two (structure **II**) of the water ligands by *n*-propylamine, thereby modeling the most probable coordination sites of the amine to $Rh_2(OAc)_4$. The chemical shifts (referenced to CH_3NO_2) calculated for the nitrogen nuclei in the three displayed structures are summarized in Table 1.

Table 1. Calculated ^{15}N chemical shifts of structures **I**–**III** and comparison with experimental ^{15}N chemical shifts from liquid-state and solid-state NMR data.

Structure	$\delta^{15}N$ calculated [ppm/CH_3NO_2]	$\delta^{15}N$ experimental liquid-state NMR [ppm/CH_3NO_2]	$\delta^{15}N$ experimental solid-state NMR [ppm/CH_3NO_2]
I	−397.5	−395.7	−402.7
II	−387.4/−388.3		
III	−363.2	−359.9	−349.0

Comparing the shift of the free amine group (structure **III**) with that of the rhodium-bound amine group in structure **I**, the upfield shift of approximately $\delta=35.8$ ppm observed in the liquid spectrum (see Supporting Information, Figure S4) is accurately reproduced. The calculated difference between the single amine coordination in structure **I** and the double coordination in structure **II** (10 ppm) is relatively small and does not allow a clear discrimination between these two possible coordination modes within the error margins of the employed B3LYP/6-311++G(3df,3dp) level of theory. For the interpretation of the chemical shifts observed in the solid-state spectra, the calculated ^{15}N values for the amine groups can only provide rough guidelines for the change in electronic structure upon coordination at rhodium. The calculated upfield shift of 35.8 ppm in the liquid-state spectrum is more marked in the solid-state spectrum, amounting to 53.7 ppm. These results strongly support the hypothesis that the dirhodium catalyst is immobilized through amine linkers.

Sensitivity enhancement by DNP

To illustrate the efficiency of the DNP-enhanced solid-state NMR approach, a ^{13}C reference spectrum for SBA-15–NH_2–COOH + $Rh_2(OAc)_4$ (**3**) was recorded by employing the same parameters but without microwave irradiation (Figure 3c). This spectrum showed no significant signals within the applied measurement time of 20 min. Compared to this spectrum, the signal-to-noise ratio of the DNP spectrum is improved by a factor of 24. This enhancement factor is comparable to the values achieved by other research groups for surface-enhanced DNP on functionalized porous silica materials.[92]

For ^{15}N, the enhancement factor was only calculated for SBA-15–NH_2 (**2**) (see Supporting Information, Figure S5), which served as a test sample for evaluation of the ^{15}N DNP set-up. Even without any optimization, an enhancement factor of about six was achieved, which corresponds to a time gain of 36 compared to the standard solid-state NMR experiment. This clearly demonstrates the high potential of ^{15}N DNP for characterizing nitrogen-containing binding sites in heterogeneous systems.

Activity test of the SBA-15–NH_2–COOH + $Rh_2(OAc)_4$ (3) catalyst

To test the catalytic application potential of the heterogeneous dirhodium catalyst (**3**), a model cyclopropanation reaction was performed employing EDA and styrene as substrates (Scheme 1). The results of this activity study are displayed graphically in Figure 6. The overall yield of the products (*cis*- and *trans*-1-ethoxycarbonyl-2-phenylcyclopropane) increased with the reaction time and reached about 55% after 5 h. During the reaction, the *cis* and *trans* isomers were produced in yields of 45% and 55%, respectively. The results confirmed the efficiency of the heterogeneous dirhodium catalyst for cyclopropanation even without optimization of the catalyst structure, and demonstrated the applicability of this catalyst for preparing precursors of pharmaceutical ingredients.

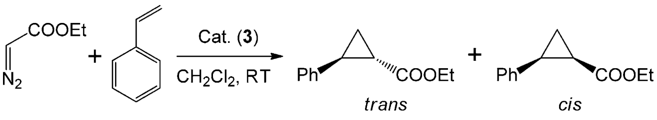

Scheme 1. Reaction scheme of the cyclopropanation of EDA with styrene according to ref. [7] catalyzed by SBA-15–NH_2–COOH + $Rh_2(OAc)_4$ (**3**).

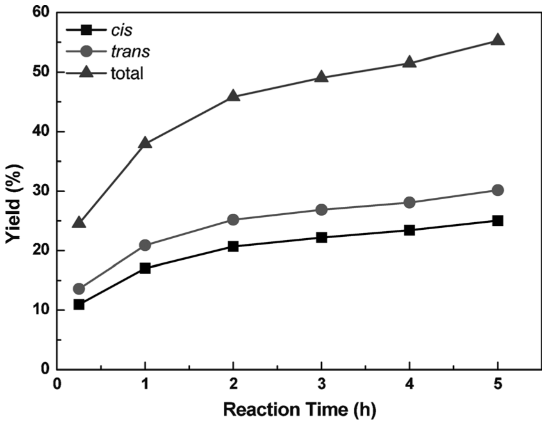

Figure 6. Overall yield of the product mixture (▲), of the *cis* isomer (■), and the *trans* isomer (●) as functions of reaction time.

Conclusions

A novel heterogeneous dirhodium catalyst based on a functionalized silica support material has been synthesized. The dirhodium acetate dimer ($Rh_2(OAc)_4$) was chosen as a model complex for grafting onto bifunctionalized mesoporous silica (SBA-15–NH_2–COOH). This catalyst has been applied in the cyclopropanation reaction of EDA with styrene, showing efficient conversion to form the *cis*- and *trans*-1-ethoxycarbonyl-2-phenylcyclopropane product at room temperature. ^{29}Si solid-state NMR has confirmed successful functionalization of the mesoporous SBA-15 material. Surface-enhanced ^{13}C CP MAS and ^{15}N CP MAS experiments allow us to distinguish the different binding sites on the support material, such as carbonyl, amine, and amide functions. These experiments have shown that both carboxyl and amine ligands facilitate strong and stable binding of the dirhodium catalyst on the surface. The interpretation of the chemical shift values for different binding sites has been corroborated by quantum chemical calculations on dirhodium model complexes, which are in excellent agreement with the experimental results. This study clearly demonstrates the high application potential of DNP NMR for detecting nuclei such as ^{15}N in natural abundance, which may be employed to distinguish different amine binding sites in heterogeneous catalyst systems on a fast time scale. Furthermore, it allows the possibility of analyzing a wide range of systems with nitrogen-containing groups that cannot be easily spin labeled.

Acknowledgements

This work has been supported by the Deutsche Forschungsgemeinschaft (DFG) under contract Bu-911-20-1, which gave us the opportunity to set up the DNP spectrometer, and Bu-911-12-2, and the Islandic Research Fund (141062-051). We further thank Bruker Biospin Germany and France for technical installation and support of the DNP spectrometer. Particular acknowledgement is given to the technicians N. Mathieu, F. Rohé, and F. Aussenac from Bruker France for their excellent technical support on the DNP. We thank Dr. R. Meusinger from the organic chemistry department (TU Darmstadt) for measuring the 2D liquid-state NMR spectra.

Keywords: dynamic nuclear polarization · heterogeneous catalysis · hyperpolarization · immobilized catalyst · NMR spectroscopy

[1] H. M. L. Davies, R. E. J. Beckwith, *Chem. Rev.* **2003**, *103*, 2861–2903.
[2] M. P. Doyle, R. Duffy, M. Ratnikov, L. Zhou, *Chem. Rev.* **2010**, *110*, 704–724.
[3] N. R. Candeias, C. A. M. Afonso, P. M. P. Gois, *Org. Biomol. Chem.* **2012**, *10*, 3357–3378.
[4] H. M. L. Davies, A. M. Walji, *Org. Lett.* **2003**, *5*, 479–482.
[5] H. M. L. Davies, A. M. Walji, *Org. Lett.* **2005**, *7*, 2941–2944.
[6] H. M. L. Davies, A. M. Walji, T. Nagashima, *J. Am. Chem. Soc.* **2004**, *126*, 4271–4280.
[7] E. V. Dikarev, D. K. Kumar, A. S. Filatov, A. Anan, Y. Xie, T. Asefa, M. A. Petrukhina, *ChemCatChem* **2010**, *2*, 1461–1466.

[8] T. Nagashima, H. M. L. Davies, *Org. Lett.* **2002**, *4*, 1989 – 1992.

[9] D. E. Bergbreiter, M. Morvant, B. Chen, *Tetrahedron Lett.* **1991**, *32*, 2731 – 2734.

[10] H. M. Hultman, M. de Lang, M. Nowotny, I. Arends, U. Hanefeld, R. A. Sheldon, T. Maschmeyer, *J. Catal.* **2003**, *217*, 264 – 274.

[11] K. Takeda, T. Oohara, M. Anada, H. Nambu, S. Hashimoto, *Angew. Chem. Int. Ed.* **2010**, *49*, 6979 – 6983; *Angew. Chem.* **2010**, *122*, 7133 – 7137.

[12] D. Brunel, N. Bellocq, P. Sutra, A. Cauvel, M. Lasperas, P. Moreau, F. Di Renzo, A. Galarneau, F. Fajula, *Coord. Chem. Rev.* **1998**, *178 – 180*, 1085 – 1108.

[13] P. Iliade, I. Miletto, S. Coluccia, G. Berlier, *Res. Chem. Intermed.* **2012**, *38*, 785 – 794.

[14] X. S. Zhao, X. Y. Bao, W. Guo, F. Y. Lee, *Mater. Today* **2006**, *9*, 32 – 39.

[15] J. O. Krause, O. Nuyken, K. Wurst, M. R. Buchmeiser, *Chem. Eur. J.* **2004**, *10*, 777 – 784.

[16] H. Brunner, E. Bielmeier, J. Wiehl, *J. Organomet. Chem.* **1990**, *384*, 223 – 241.

[17] J. Evans, A. B. Zaki, M. Y. El-Sheikh, S. A. El-Safty, *J. Phys. Chem. B* **2000**, *104*, 10271 – 10281.

[18] C. Merckle, S. Haubrich, J. Bluemel, *J. Organomet. Chem.* **2001**, *627*, 44 – 54.

[19] H. Werner, U. Mohring, *J. Organomet. Chem.* **1994**, *475*, 277 – 282.

[20] A. J. Sandee, J. N. H. Reek, P. C. J. Kamer, P. W. N. M. van Leeuwen, *J. Am. Chem. Soc.* **2001**, *123*, 8468 – 8476.

[21] W. H. Cheung, W. Y. Yu, W. P. Yip, N. Y. Zhu, C. M. Che, *J. Org. Chem.* **2002**, *67*, 7716 – 7723.

[22] H. L. Li, N. Perkas, Q. L. Li, Y. Gofer, Y. Koltypin, A. Gedanken, *Langmuir* **2003**, *19*, 10409 – 10413.

[23] A. Crosman, W. E. Hoelderich, *J. Catal.* **2005**, *232*, 43 – 50.

[24] C. Merckle, J. Bluemel, *Top. Catal.* **2005**, *34*, 5 – 15.

[25] A. M. J. Rost, H. Schneider, J. P. Zoller, W. A. Herrmann, F. E. Kuhn, *J. Organomet. Chem.* **2005**, *690*, 4712 – 4718.

[26] N. K. K. Raj, S. S. Deshpande, R. H. Ingle, T. Raja, P. Manikandan, *Stud. Surf. Sci. Catal.* **2005**, *156*, 769 – 778.

[27] P. M. Rao, A. Wolfson, S. Kababya, S. Vega, M. V. Landau, *J. Catal.* **2005**, *232*, 210 – 225.

[28] J. Kasai, Y. Nakagawa, S. Uchida, K. Yamaguchi, N. Mizuno, *Chem. Eur. J.* **2006**, *12*, 4176 – 4184.

[29] T. Posset, J. Bluemel, *J. Am. Chem. Soc.* **2006**, *128*, 8394 – 8395.

[30] F. Hoffmann, M. Cornelius, J. Morell, M. Froba, *J. Nanosci. Nanotechnol.* **2006**, *6*, 265 – 288.

[31] M. Heitbaum, F. Glorius, I. Escher, *Angew. Chem. Int. Ed.* **2006**, *45*, 4732 – 4762; *Angew. Chem.* **2006**, *118*, 4850 – 4881.

[32] T. Joseph, S. S. Deshpande, S. B. Halligudi, A. Vinu, S. Ernst, M. Hartmann, *J. Mol. Catal. A* **2003**, *206*, 13 – 21.

[33] S. Shylesh, S. Sharma, S. P. Mirajkar, A. P. Singh, *J. Mol. Catal.* **2004**, *212*, 219 – 228.

[34] A. Grünberg, Y. P. Xu, H. Breitzke, G. Buntkowsky, *Chem. Eur. J.* **2010**, *16*, 6993 – 6998.

[35] M. Yang, F. F. Xu, C. Wang, X. M. Liu, P. F. Yan, P. P. Li, U. Welz-Biermann, *Eur. J. Inorg. Chem.* **2012**, 4500 – 4506.

[36] M. Colilla, I. Izquierdo-Barba, S. Sánchez-Salcedo, J. L. G. Fierro, J. L. Hueso, M. Vallet-Regí, *Chem. Mater.* **2010**, *22*, 6459 – 6466.

[37] M. W. McKittrick, C. W. Jones, *J. Catal.* **2004**, *227*, 186 – 201.

[38] J. L. Rapp, Y. Huang, M. Natella, Y. Cai, V. S. Y. Lin, M. Pruski, *Solid State Nucl. Magn. Reson.* **2009**, *35*, 82 – 86.

[39] A. Adamczyk, Y. Xu, B. Walaszek, F. Roelofs, T. Pery, K. Pelzer, K. Philippot, B. Chaudret, H. H. Limbach, H. Breitzke, G. Buntkowsky, *Top. Catal.* **2008**, *48*, 75 – 83.

[40] J. Blümel, *Coord. Chem. Rev.* **2008**, *252*, 2410 – 2423.

[41] A. Grünberg, H. Breitzke, G. Buntkowsky, *Spectroscopic Properties of Inorganic and Organometallic Compounds: Techniques, Materials and Applications, Vol 43*, **2012**, pp. 289 – 323.

[42] J. Blümel, *Nachr. Chem.* **2006**, *54*, 632 – 638.

[43] T. Iwai, R. Tanaka, T. Harada, M. Sawamura, *Chem. Eur. J.* **2014**, *20*, 1057 – 1065.

[44] S. Sánchez-Salcedo, M. Colilla, I. Izquierdo-Barba, M. Vallet-Regi, *J. Mater. Chem. B* **2013**, *1*, 1595 – 1606.

[45] G. Wu, R. E. Wasylishen, *Organometallics* **1992**, *11*, 3242 – 3248.

[46] G. Wu, R. E. Wasylishen, *J. Chem. Phys.* **1993**, *98*, 6138 – 6149.

[47] G. Wu, R. E. Wasylishen, *Inorg. Chem.* **1996**, *35*, 3113 – 3116.

[48] K. Mao, J. W. Wiench, V. S. Y. Lin, M. Pruski, *J. Magn. Reson.* **2009**, *196*, 92 – 95.

[49] J. W. Wiench, C. Michon, A. Ellern, P. Hazendonk, A. Iuga, R. J. Angelici, M. Pruski, *J. Am. Chem. Soc.* **2009**, *131*, 11801 – 11810.

[50] A. Grünberg, T. Gutmann, N. Rothermel, Y. Xu, H. Breitzke, G. Buntkowsky, *Z. Phys. Chem. (Muenchen Ger.)* **2013**, *227*, 901 – 915.

[51] T. Gutmann, A. Gruenberg, N. Rothermel, M. Werner, M. Srour, S. Abdulhussain, S. Tan, Y. Xu, H. Breitzke, G. Buntkowsky, *Solid State Nucl. Magn. Reson.* **2013**, *55 – 56*, 1 – 11.

[52] S. S. Arzumanov, A. G. Stepanov, *J. Phys. Chem. C* **2013**, *117*, 2888 – 2892.

[53] H. Henning, M. Dyballa, M. Scheibe, E. Klemm, M. Hunger, *Chem. Phys. Lett.* **2013**, *555*, 258 – 262.

[54] "Parahydrogen-Induced Polarization in Heterogeneous Catalytic Processes": K. V. Kovtunov, V. V. Zhivonitko, I. V. Skovpin, D. A. Barskiy, I. V. Koptyug, in *Topics in Current Chemistry Vol. 338*, **2013**, pp. 123 – 180.

[55] A. A. Lysova, I. V. Koptyug, *Chem. Soc. Rev.* **2010**, *39*, 4585 – 4601.

[56] J. L. Bonardet, J. Fraissard, A. Gedeon, M. A. Springuel-Huet, *Catal. Rev. Sci. Eng.* **1999**, *41*, 115 – 225.

[57] E. Brunner, *Concepts Magn. Reson.* **1999**, *11*, 313 – 335.

[58] W. Happer, E. Miron, S. Schaefer, D. Schreiber, W. A. van Wijngaarden, X. Zeng, *Phys. Rev. A* **1984**, *29*, 3092 – 3110.

[59] Y. Liu, W. Zhang, X. Han, X. Bao, *Chin. J. Catal.* **2006**, *27*, 827 – 836.

[60] A. J. Rossini, A. Zagdoun, M. Lelli, A. Lesage, C. Copéret, L. Emsley, *Acc. Chem. Res.* **2013**, *46*, 1942 – 1951.

[61] T. Maly, G. T. Debelouchina, V. S. Bajaj, K. N. Hu, C. G. Joo, M. L. Mak-Jurkauskas, J. R. Sirigiri, P. C. A. van der Wel, J. Herzfeld, R. J. Temkin, R. G. Griffin, *J. Chem. Phys.* **2008**, *128*, 052211.

[62] T. Kobayashi, O. Lafon, A. S. Lilly Thankamony, I. I. Slowing, K. Kandel, D. Carnevale, V. Vitzthum, H. Vezin, J.-P. Amoureux, G. Bodenhausen, M. Pruski, *Phys. Chem. Chem. Phys.* **2013**, *15*, 5553 – 5562.

[63] U. Akbey, B. Altin, A. Linden, S. Ozcelik, M. Gradzielski, H. Oschkinat, *Phys. Chem. Chem. Phys.* **2013**, *15*, 20706 – 20716.

[64] A. J. Rossini, A. Zagdoun, M. Lelli, J. Canivet, S. Aguado, O. Ouari, P. Tordo, M. Rosay, W. E. Maas, C. Copéret, D. Farrusseng, L. Emsley, A. Lesage, *Angew. Chem. Int. Ed.* **2012**, *51*, 123 – 127; *Angew. Chem.* **2012**, *124*, 127 – 131.

[65] W. R. Grüning, A. J. Rossini, A. Zagdoun, D. Gajan, A. Lesage, L. Emsley, C. Copéret, *Phys. Chem. Chem. Phys.* **2013**, *15*, 13270 – 13274.

[66] L. Zhao, W. Li, A. Plog, Y. Xu, G. Buntkowsky, T. Gutmann, K. Zhang, *Phys. Chem. Chem. Phys.* **2014**, *16*, 26322 – 26329.

[67] F. Blanc, S. Y. Chong, T. O. McDonald, D. J. Adams, S. Pawsey, M. A. Caporini, A. I. Cooper, *J. Am. Chem. Soc.* **2013**, *135*, 15290 – 15293.

[68] A. Zagdoun, G. Casano, O. Ouari, G. Lapadula, A. J. Rossini, M. Lelli, M. Baffert, D. Gajan, L. Veyre, W. E. Maas, M. Rosay, R. T. Weber, C. Thieuleux, C. Copéret, A. Lesage, P. Tordo, L. Emsley, *J. Am. Chem. Soc.* **2012**, *134*, 2284 – 2291.

[69] M. Rosay, J. C. Lansing, K. C. Haddad, W. W. Bachovchin, J. Herzfeld, R. J. Temkin, R. G. Griffin, *J. Am. Chem. Soc.* **2003**, *125*, 13626 – 13627.

[70] G. T. Debelouchina, M. J. Bayro, P. C. A. van der Wel, M. A. Caporini, A. B. Barnes, M. Rosay, W. E. Maas, R. G. Griffin, *Phys. Chem. Chem. Phys.* **2010**, *12*, 5911 – 5919.

[71] I. Gelis, V. Vitzthum, N. Dhimole, M. A. Caporini, A. Schedlbauer, D. Carnevale, S. R. Connell, P. Fucini, G. Bodenhausen, *J. Biomol. NMR* **2013**, *56*, 85 – 93.

[72] V. S. Bajaj, M. L. Mak-Jurkauskas, M. Belenky, J. Herzfeld, R. G. Griffin, *J. Magn. Reson.* **2010**, *202*, 9 – 13.

[73] I. Izquierdo-Barba, S. Sánchez-Salcedo, M. Colilla, M. J. Feito, C. Ramírez-Santillán, M. T. Portolés, M. Vallet-Regí, *Acta Biomater.* **2011**, *7*, 2977 – 2985.

[74] K. N. Hu, C. Song, H. H. Yu, T. M. Swager, R. G. Griffin, *J. Chem. Phys.* **2008**, *128*, 052302.

[75] C. S. Song, K. N. Hu, C. G. Joo, T. M. Swager, R. G. Griffin, *J. Am. Chem. Soc.* **2006**, *128*, 11385 – 11390.

[76] A. E. Bennett, C. M. Rienstra, M. Auger, K. V. Lakshmi, R. G. Griffin, *J. Chem. Phys.* **1995**, *103*, 6951.

[77] S. Hayashi, K. Hayamizu, *Bull. Chem. Soc. Jpn.* **1991**, *64*, 688 – 690.

[78] F. Neese, *Wiley Interdiscip. Rev. Comput. Mol. Sci.* **2012**, *2*, 73 – 78.

[79] F. A. Cotton, B. G. de Boer, M. D. Laprade, J. R. Pipal, D. A. Ucko, *Acta Crystallogr. Sect. B* **1971**, *27*, 1664 – 1671.

[80] A. D. Becke, *J. Chem. Phys.* **1993**, *98*, 1372 – 1377.

[81] A. D. Becke, *J. Chem. Phys.* **1993**, *98*, 5648 – 5652.

[82] C. T. Lee, W. T. Yang, R. G. Parr, *Phys. Rev. B* **1988**, *37*, 785 – 789.
[83] W. J. Hehre, R. Ditchfield, J. A. Pople, *J. Chem. Phys.* **1972**, *56*, 2257.
[84] J. D. Dill, J. A. Pople, *J. Chem. Phys.* **1975**, *62*, 2921 – 2923.
[85] K. A. Peterson, D. Figgen, M. Dolg, H. Stoll, *J. Chem. Phys.* **2007**, *126*, 124101.
[86] T. Clark, J. Chandrasekhar, G. W. Spitznagel, P. von R. Schleyer, *J. Comput. Chem.* **1983**, *4*, 294 – 301.
[87] M. J. Frisch, J. A. Pople, J. S. Binkley, *J. Chem. Phys.* **1984**, *80*, 3265 – 3269.
[88] R. Krishnan, J. S. Binkley, R. Seeger, J. A. Pople, *J. Chem. Phys.* **1980**, *72*, 650 – 654.
[89] S. Abdulhussain, H. Breitzke, T. Ratajczyk, A. Gruenberg, M. Srour, D. Arnaut, H. Weidler, U. Kunz, H. J. Kleebe, U. Bommerich, J. Bernarding, T. Gutmann, G. Buntkowsky, *Chem. Eur. J.* **2014**, *20*, 1159 – 1166.
[90] V. Schimming, C.-G. Hoelger, G. Buntkowsky, I. Sack, J.-H. Fuhrhop, S. Rocchetti, H. H. Limbach, *J. Am. Chem. Soc.* **1999**, *121*, 4892 – 4893.
[91] A. Sayari, A. Heydari-Gorji, Y. Yang, *J. Am. Chem. Soc.* **2012**, *134*, 13834 – 13842.
[92] O. Lafon, A. S. L. Thankamony, T. Kobayashi, D. Carnevale, V. Vitzthum, I. I. Slowing, K. Kandel, H. Vezin, J. P. Amoureux, G. Bodenhausen, M. Pruski, *J. Phys. Chem. C* **2013**, *117*, 1375 – 1382.

Received: August 29, 2014